Article

Performance Evaluation of an Anti-Lock Braking System for Electric Vehicles with a Fuzzy Sliding Mode Controller

Jingang Guo *, Xiaoping Jian and Guangyu Lin

School of Automobile, Chang'an University, Xi'an 710061, Shaanxi, China;
E-Mails: jxp@chd.edu.cn (X.J.); lsgyu@chd.edu.cn (G.L.)

* Author to whom correspondence should be addressed; E-Mail: guojg@chd.edu.cn;
Tel.: +86-29-8233-4430; Fax: +86-29-8233-4476.

Abstract: Traditional friction braking torque and motor braking torque can be used in braking for electric vehicles (EVs). A sliding mode controller (SMC) based on the exponential reaching law for the anti-lock braking system (ABS) is developed to maintain the optimal slip value. Parameter optimizing is applied to the reaching law by fuzzy logic control (FLC). A regenerative braking algorithm, in which the motor torque is taken full advantage of, is adopted to distribute the braking force between the motor braking and the hydraulic braking. Simulations were carried out with Matlab/Simulink. By comparing with a conventional Bang-bang ABS controller, braking stability and passenger comfort is improved with the proposed SMC controller, and the chatting phenomenon is reduced effectively with the parameter optimizing by FLC. With the increasing proportion of the motor braking torque, the tracking of the slip ratio is more rapid and accurate. Furthermore, the braking distance is shortened and the conversion energy is enhanced.

Keywords: electric vehicle (EV); anti-lock braking system (ABS); sliding mode control; fuzzy logic control

1. Introduction

The anti-lock braking system (ABS) is the most important active safety system for road vehicles. The ABS can greatly improve the safety of a vehicle in extreme circumstances since the ABS can maximize the longitudinal tire-road friction while keeping large lateral (directional) forces that ensure vehicle drive-ability [1]. At present, the ABS has become standard equipment for all new passenger cars in many countries.

As a key technology, regenerative braking is an effective approach to improve vehicle efficiency, and has been applied in various types of electric vehicles (EVs). However, the conventional friction braking system must be retained and works together with the regenerative braking system since the regenerative braking torque is limited by many factors, such as the motor speed, the state of charge (*SOC*) and temperature of the battery [2]. This prompts the development and investigation of regenerative braking strategies and control methods during normal braking events and emergency braking events [3,4].

Tur *et al.* [5] proposed a method that employed pure regenerative braking force with proportion-integral-differential (PID) control when the ABS works. The simulation results with a quarter vehicle model showed that the regenerative ABS response is better for panic stop situations. Bera *et al.* [6] discussed a bond graph model of a vehicle with the ABS and regenerative braking module, and a sliding mode controller (SMC) for ABS was developed. Based on a motor priority distribution algorithm, the braking force was distributed between the regenerative braking and the antilock braking in emergency/panic braking situations. Simulations showed that with combined regenerative and antilock braking, the vehicle's safety and energy efficiency both increases. Peng *et al.* [2] put forward a fuzzy logic control (FLC) strategy for a regenerative braking and antiskid braking system for hybrid EVs (HEVs), and the coordinative control between the regenerative and hydraulic braking were developed. Simulation and experimental results showed that vehicle braking performance and fuel economy can be improved and the proposed control strategy and method are effective and robust.

As is well known, the control of the ABS is complicated. The main difficulty arising in the design of the ABS control is the strong nonlinearity and uncertainty. Standard ABS systems for wheeled vehicles equipped with traditional hydraulic actuators mainly use rule-based control logics. In recent years, technological advances in actuators have led to both electro-hydraulic and electro-mechanical braking (EMB) systems, which enable a continuous modulation of the braking torque [1]. As a device with fast torque response, the advantage of the motor as an actuator has been realized by more and more researchers. A number of advanced control approaches have been proposed for the ABS, such as FLC [7], neural network [8], adaptive control [9], and other intelligent control.

As actuator of anti-skid control, Sakai *et al.* [10] compared the electric motor with the hydraulic brake system, and the advantage of the electric motor as an actuator is clarified by simulations considering the delay of actuator response. Mi *et al.* [11] presented an iterative learning control for the ABS on various road conditions. Only the electric motor in HEVs and EVs propulsion systems was used to achieve antilock braking performance. Through an iterative learning process, the motor torque was optimized to keep the tire slip ratio corresponding to the peak traction coefficient during braking. Zhou *et al.* [12] proposed a coordinated control of regenerative braking and EMB for a parallel HEV (PHEV), and studied antilock braking control of the EMB to maintain safety and stability of the vehicle using sliding-mode control. To reduce the vibrations induced by the controller, FLC was used

to adjust the switching gain of sliding-mode control. Simulation results indicated that the fuzzy-sliding mode control can keep the real slip ratio following the optimal slip ratio closely and quickly.

SMC is a variable structure control. SMC has been popularized in many fields for its robust performance against time-dependent parameter variations, disturbances, and simplicity of physical realization [13]. This is very suitable for ABS control. In this paper, a sliding-mode methodology has been adopted to design the ABS control of a front drive EV. For the drawback of high-frequency chattering generated by the conventional sliding mode control, a method of parameter fuzzy optimization for exponential approach law is proposed, which can meet the requirements for small chattering, strong disturbance attenuation and fast convergence. To maximize the use of the regenerative brake torque, the algorithm of braking force distribution keeps the hydraulic friction brake torque to its minimum. Simulation results show the validity and the effectiveness of the fuzzy SMC. The contribution of the paper includes three aspects: (a) a sliding-mode methodology based on exponential reaching law has been adopted to design the ABS controller; (b) FLC is applied to optimize the parameter of the exponential reaching law; and (c) a distribution algorithm that the motor torque is taken full advantage is adopted to distribute the braking torque between the motor and the hydraulic braking system.

This paper is organized as follows: Section 2 describes the structure of the braking system investigated in this paper and system modeling, including the three degrees of freedom (3-DOF) longitudinal vehicle model, the Burckhardt tire model, an experimental motor model and a hydraulic brake system model; in Section 3, a SMC based on exponential reaching law for ABS is developed and the FLC is adopted to optimize the parameter of the exponential reaching law; the regenerative braking algorithm is introduced in Section 4; then simulations are performed in Section 5. The comparisons of performance of ABS with a Bang-bang controller and the proposed SMC controller, with and without the optimizing parameter, and the distribution of braking force using different actuator, are carried out with Matlab/Simulink.

2. System Modeling

The structure of the braking system investigated in this paper is shown in Figure 1. The vehicle is considered to have front wheel drive. The motor braking torque is applied to the front wheel through the transmission. The hydraulic brake system consists of a brake pedal, a vacuum booster, a master cylinder, a hydraulic control unit and four wheel cylinders and wheel speed sensors. Wheel speed sensors are mounted on the wheels to measure the wheel speeds and send signals to the brake control unit. When the brake is applied, the brake control unit calculates the required braking torque on the front and rear wheels according to the brake pedal stroke, and estimates the available motor braking torque according to vehicle velocity, battery *SOC* and other information. On the base of the braking torque distribution algorithm, the demand motor torque is determined, and the brake control unit sends command signals to the motor control unit. The motor control unit controls the motor work or not to meet the demand on the motor torque, and transmits the actual motor braking torque signals to the brake control unit. The friction braking torque applied to the front wheel is determined by the difference of the required braking torque to the front wheel and the actual motor braking torque. Simultaneously, through the vacuum booster, the master cylinder and the proportional valve, the hydraulic

pressure supplied by the brake pedal force is transmitted to the rear wheel cylinders, generating braking torque to the rear wheel.

Figure 1. Configuration of the braking control system.
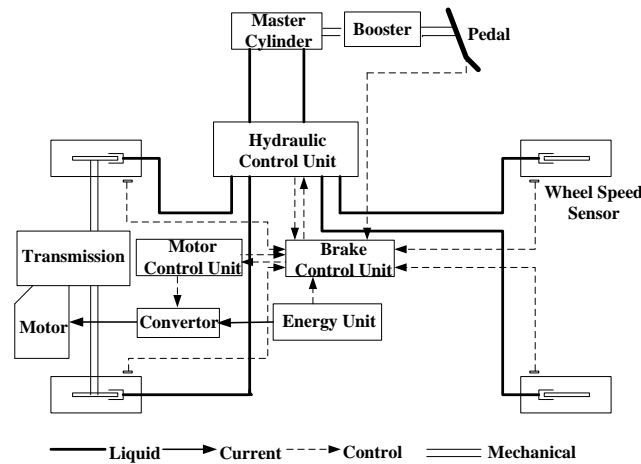
2.1. Vehicle Model

In this paper, only straight-line braking is considered. For the testing of braking control algorithm, a simple but effective model known as the 3-DOF longitudinal vehicle model is used. The main feature of this model is that it can describe the load transfer phenomena. The 3-DOF consists of the longitudinal velocity, the front wheel angular speed, and the rear wheel angular speed. It is worth noting that, in addition to the torque exerted by traditional friction braking system, motor braking torque will also be used on the front wheel since a front-drive EV is studied.

During braking, the dynamic equations [14] are described as:

$$m\dot{v} = -(F_{bf} + F_{br} + F_{a} + F_{f}) \tag{1}$$

$$J_{\omega f}\,\dot{\omega}_{f} = F_{bf} \cdot R - T_{hf} - T_{mf} - T_{ff} \tag{2}$$

$$J_{\omega r}\,\dot{\omega}_{r} = F_{br} \cdot R - T_{hr} - T_{fr} \tag{3}$$

where m is the vehicle mass; $\dot{v}$ is the vehicle velocity; F_{bf} and F_{br} are the braking forces of the front and rear axles, respectively; F_{a} is the aerodynamic resistance, $F_{a} = C_{a}v^2$ (C_{a} is a constant decided by body style) when the wind speed is ignored; F_{f} is the rolling resistance; $J_{\omega f}$ and $J_{\omega r}$ are the inertia moment of the front and rear wheels, respectively; $\dot{\omega}_{f}$ and $\dot{\omega}_{r}$ are the angular speed of the front and rear wheels, respectively; R is the radius of the wheel; T_{hf} and T_{hr} are the hydraulic braking torque applied on the front wheel and rear wheel; T_{ff} and T_{fr} are the rolling resistance torque on the front wheel and rear wheel; and T_{mf} is the motor braking torque on the front wheel.

During braking, considering load transfer from the rear axle to the front axle, the normal loads on the front and rear axles can be expressed as:

$$\begin{cases} F_{zf} = \dfrac{1}{L}[WL_{r} - h_{g}(m\dot{v} + F_{a})] \\[2mm] F_{zr} = \dfrac{1}{L}[WL_{f} + h_{g}(m\dot{v} + F_{a})] \end{cases} \tag{4}$$

where F_{zf} and F_{zr} are the normal loads on the front and rear axles, respectively; W is the vehicle weight; L is the wheelbase; h_g is the height of the center of mass from the ground; L_f and L_r are the distance between the front axle and the rear axle to the center of mass, respectively.

The braking force developed on the tire-road interface is determined by the normal load and the braking effort coefficient of road adhesion. The braking force on the front and rear axles are given by:

$$\begin{cases} F_{bf} = \mu F_{zf} = \mu \dfrac{1}{L}[WL_r - h_g(m\dot{v} + F_a)] \\ F_{br} = \mu F_{zr} = \mu \dfrac{1}{L}[WL_f + h_g(m\dot{v} + F_a)] \end{cases} \tag{5}$$

where μ is the braking effort coefficient of road adhesion.

2.2. Tire Model

The tire connects the external torques with the vehicle's longitudinal motion. The tire model includes empirical (semiempirical) and analytical models. Several models describing the nonlinear behavior of the tire have been reported in the literature, such as Magic Formula [15], LuGre tire model, and so on. In this paper, the Burckhardt model [16] will be used, as it is particularly suitable for analytical purpose while retaining a good degree of accuracy in the description of the friction coefficient.

During braking, the longitudinal slip ratio is defined as:

$$\lambda = \frac{v - \omega R}{v} \tag{6}$$

where λ is the slip ratio; and ω is the angular speed of the wheel.

Based on Burckhardt model, the velocity dependent braking effort coefficient between the tire and the road has the following form:

$$\mu(\lambda, v) = [C_1(1 - e^{-C_2\lambda}) - C_3\lambda]e^{-C_4\lambda v} \tag{7}$$

where C_1 is the maximum value of friction curve; C_2 is the friction curve shape; C_3 is the friction curve difference between the maximum value and the value at $\lambda = 1$; and C_4 is wetness characteristic value. By changing the values of parameters C_1–C_4, many different tire-road friction conditions can be modeled. The parameters for different road surfaces are listed in Table 1.

Table 1. Tire-road friction parameters.

| Surface conditions	C_1	C_2	C_3	C_4
Dry asphalt	1.029	17.16	0.523	0.03
Dry concrete	1.1973	25.168	0.5373	0.03
Snow	0.1946	94.129	0.0646	0.03
Ice	0.05	306.39	0	0.03

In Figure 2, the shapes of braking effort coefficient for four different road conditions with a vehicle velocity of 10 m/s are displayed.

When a tire is locked, the braking effort coefficient falls to its sliding value. As a result, the vehicle will lose directional control and stability. The prime function of an antilock brake system is to prevent the tire from locking and ideally to keep the skid of the tire within a desired range.

Figure 2. Slip-friction curves for different road conditions.
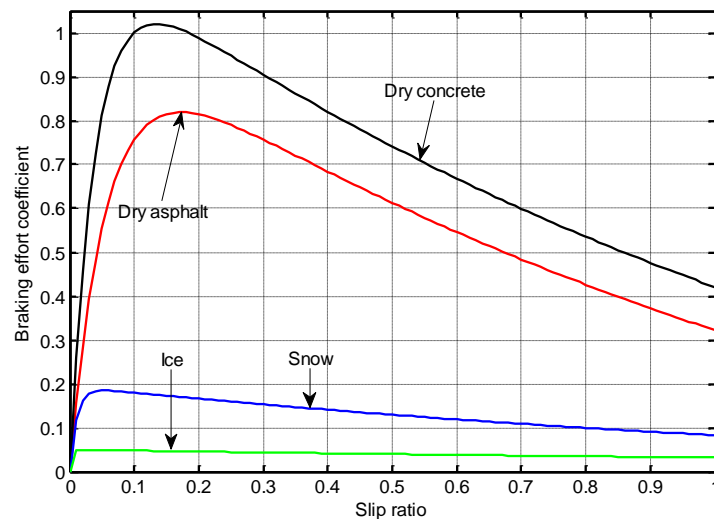
2.3. Motor Model

In driving mode, the motor is used as an actuator. However, in the regenerative braking mode, it functions as a generator. The fast torque response characteristics of the motor provide the opportunity to improve the vehicle antilock performance. In this paper, an experimental motor model of a 32 kW permanent magnet synchronous motor from the Advanced Vehicle Simulator (ADVISOR) Database [17] will be used. The motor model uses lookup table for defining the torque and efficiency characteristics. Figure 3 shows the maximum torque-speed curve and the efficiency map of the motor at various operating points.

Figure 3. Motor torque-speed curve and efficiency map.
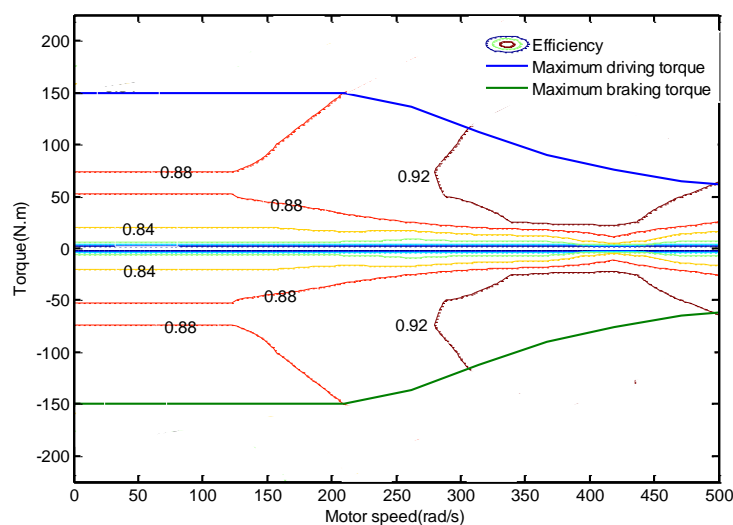
During braking, in view of the motor efficiency, the conversion energy by the motor is obtained as:

$$E = \int (T_{\mathrm{m}} \cdot \omega_{\mathrm{m}} \cdot \eta_{\mathrm{reg}}) \mathrm{d}t \tag{8}$$

where T_{m} is the motor braking torque; ω_{m} is the motor angular speed; and η_{reg} is the motor efficiency when braking.

As we known, several factors have influence on the regenerative braking torque exerted by the motor. These factors mainly include battery *SOC*, motor angular speed and motor temperature [2]. The impact of motor temperature will be ignored in this paper.

The aim of considering battery *SOC* is to protect the battery from overcharging that may affect the battery life. A weight factor k_{SOC} related to *SOC* is introduced and defined as:

$$k_{SOC} = \begin{cases} 1 & SOC \leq 0.8 \\ 10(0.9 - SOC) & 0.8 < SOC \leq 0.9 \\ 0 & 0.9 < SOC \leq 1 \end{cases} \tag{9}$$

The influence of motor angular speed mainly comes from the very low electric motive force (voltage) generated at low motor rotational speed. Similarly, the weight factor k_{ω_m} as follow is used:

$$k_{\omega_m} = \begin{cases} 0 & \omega_m \leq 50 \text{ rad/s} \\ (\omega_m - 50)/50 & 50 < \omega_m \leq 100 \text{ rad/s} \\ 1 & \omega_m > 100 \text{ rad/s} \end{cases} \tag{10}$$

After the battery *SOC* and the motor angular speed are taken into account, the available motor braking torque is obtained as:

$$T_{mavail} = \frac{T_{mmax} \cdot i \cdot k_{\omega_m} \cdot k_{SOC}}{\eta_t} \tag{11}$$

where T_{mavail} is the available motor braking torque applied at the wheel; T_{mmax} is the maximum motor torque, which is related to the motor speed, as shown in Figure 3; *i* is the transmission ratio; and η_t is the transmission efficiency.

When the motor is functioning as an actuator, the motor torque dynamics is very fast compared with hydraulic system. In simulation, the motor torque dynamics is modeled as a first-order system [10] as:

$$\frac{T_m}{T_{m\_demand}} = e^{-\tau_D s} \frac{1}{1 + \tau_m s} \tag{12}$$

where T_{m_demand} is the demand motor torque; τ_D is the delay constant; and τ_m is the motor torque time constant.

2.4. Hydraulic Brake System

In this paper, a hydraulic brake system as shown in Figure 4 is used. The braking torque on each wheel depends on the hydraulic pressure of wheel cylinder. In addition, the hydraulic pressure of wheel cylinder can be changed through the coordinative control of the inlet valve and the outlet valve. When the inlet valve is open and the outlet valve is closed, the pressure of wheel cylinder is increasing, and when the inlet valve is closed and the outlet valve is open, the pressure of wheel cylinder will decrease. If the both valves are closed, the brake pressure will be hold. In fact, the operation of an antilock braking system is a constantly switching process of three brake pressure. As can be seen in Figure 4, the wheel cylinder will necessarily be connected to master cylinder with brake pipes. Therefore, a transport time delay between the demand and the actual brake pressure inevitable exist in the hydraulic line. Of course, the hydraulic circuitry is only one reason that causes the delay, and another reason is the dead time of the solenoid [10]. There is no doubt that the delay will limit the performance of the actuation.

Contrary to the hydraulic brake system, the time response of the motor is quite fast, and the torque control is very precisely, which will improve the vehicle antilock function. The performance of the electric motor with hydraulic brake system as an actuator of antilock brake system is compared in [10]. Now, the studies on the antilock brake system with the electric motor as actuators are becoming more and more popular.

Figure 4. Anti-lock braking system (ABS) hydraulic brake system.
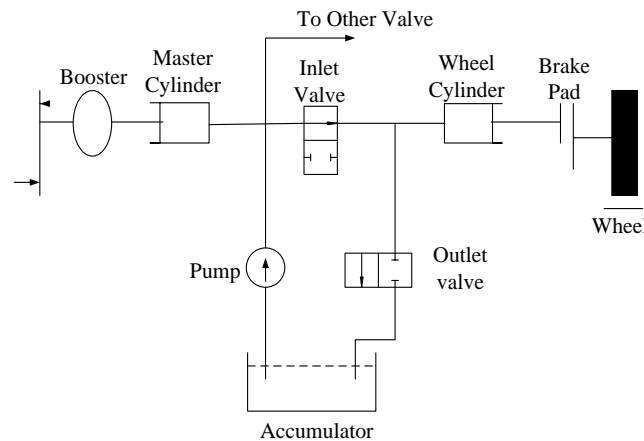
In the next part of this paper, the dynamic model of hydraulic fluid lag of brake system is used as the following first order transfer function:

$$G(s) = \frac{k}{\tau \cdot s + 1}$$

(13)

where *k* is the gain of the hydraulic system; and *τ* is the hydraulic torque time constant.

3. Sliding Mode Controller-Based Anti-Lock Braking System Controller

The objective of the ABS controller is to adjust braking torque so that the wheel slip can track the target slip ratio. In order to improve ABS performance, the control variable must have high frequency of altering. As a variable structure control, sliding mode control is a high-speed switching feedback control that switches between two values based upon some rule, which is suitable for the ABS control.

3.1. Sliding Mode Controller

The sliding mode design approach consists of two components. The first involves designing a sliding surface so that the sliding motion satisfies design specifications. The second is concerned with constructing a switched feedback gains necessary to drive the plant's state trajectory to the sliding surface. These constructions are built on the generalized Lyapunov stability theory. Note that this control law is not necessarily discontinuous.

Equations (1)–(3) can be rewritten as:

$$\dot{v} = -\frac{1}{m}\left(\sum F_{bj} + F_a + F_f\right)$$

(14)

$$\dot{\omega}_i = \frac{1}{J_{\omega i}}(F_{bi}R - T_{bi} - T_{fi})$$

(15)

where $i = f$ or r and $j = f$ or r, denoting the variable of front or rear wheel; T_{bi} is the braking torque applied by brake system, for the front wheel, $T_{bi} = T_{hf} + T_{mf}$, for the rear wheel, $T_{bi} = T_{hr}$.

The slip ratio is expressed as:

$$\lambda_i = \frac{v - \omega_i R}{v} = 1 - \frac{\omega_i R}{v} \tag{16}$$

The differentiation of Equation (16) is:

$$\dot{\lambda}_i = -\frac{R\dot{\omega}_i}{v} + \frac{R\omega_i \cdot \dot{v}}{v^2} \tag{17}$$

Inserting Equations (14) and (15) into Equation (17), we can obtain:

$$\dot{\lambda}_i = \frac{R}{J_{\omega i}}\frac{1}{v}T_{bi} + \frac{R}{J_{\omega i}}\frac{1}{v}T_{fi} - \frac{R^2}{J_{\omega i}}\frac{1}{v}F_{bi} - \frac{R\omega_i}{v^2}\frac{1}{m}\sum F_{bj} - \frac{R\omega_i}{m}\cdot C_a - \frac{R\omega_i}{mv^2}F_f \tag{18}$$

As shown in Figure 2, the braking effort coefficient varies significantly depending on the road condition. The goal of the ABS is to take full advantage of the peak braking effort coefficient, which can be achieved by maintaining the slip ratio between 0.15 and 0.25. Although the direct slip ratio measurement is difficult, many researchers have proposed various algorithms about the estimation of the slip ratio [18,19].

In order to have the slip ratio λ_i track the desired slip ratio λ_{des}, the sliding surface will be defined as:

$$S = \lambda_{des} - \lambda_i \tag{19}$$

As we know, SMC has good anti-jamming performance. The advantage of SMC is strong robustness, that is to say, it is excellently insensitive to model error and parameters change of controlled object and external disturbance. However, the disadvantage of the SMC is its chattering problem, which is caused by inherent discrete characteristic. Although the chattering can be weakened generally by controlling the speed of state variables close to sliding mode switching plane, the chattering cannot be essentially eliminated. In order to reduce the frequency of the chattering, an exponential approach law is adopted. For a continuous time system, the commonly used exponential approach law is:

$$\dot{S} = -\varepsilon \operatorname{sgn}(S) - kS \qquad \varepsilon > 0, k > 0 \tag{20}$$

where ε and k are positive constants; and $\operatorname{sgn}(S)$ is a sign function, which is defined as:

$$\operatorname{sgn}(S) = \begin{cases} 1 & S > 0 \\ -1 & S < 0 \end{cases} \tag{21}$$

Differentiating Equation (19) and substituting Equations (18) and (20) into it result in:

$$\dot{\lambda}_{des} - \frac{R}{J_{\omega i}}\frac{1}{v}T_{bi} - \frac{R}{J_{\omega i}}\frac{1}{v}T_{fi} + \frac{R^2}{J_{\omega i}}\frac{1}{v}F_{bi} + \frac{R\omega_i}{v^2}\frac{1}{m}\sum F_{bj} + \frac{R\omega_i}{m}\cdot C_a + \frac{R\omega_i}{mv^2}F_f = -\varepsilon \operatorname{sgn}(S) - kS \tag{22}$$

Therefore, the control input T_{bi} is obtained as:

$$T_{bi} = \frac{J_{\omega i}v}{R}\dot{\lambda}_{des} - T_{fi} + RF_{bi} + \frac{J_{\omega i}\omega_i}{mv}\sum F_{bj} + \frac{J_{\omega i}\omega_i v}{m}\cdot C_a + \frac{J_{\omega i}\omega_i}{mv}F_f + \frac{J_{\omega i}v}{R}\left[\varepsilon \operatorname{sgn}(\lambda_{des} - \lambda_i) + k(\lambda_{des} - \lambda_i)\right] \tag{23}$$

If the desired slip ratio λ_{des} is a constant, then the control law becomes:

$$T_{bi} = -T_{fi} + RF_{bi} + \frac{J_{\omega i}\omega_i}{m v}\sum F_{bj} + \frac{J_{\omega i}\omega_i v}{m}\cdot C_a + \frac{J_{\omega i}\omega_i}{m v}F_f + \frac{J_{\omega i}v}{R}\left[\varepsilon\,\mathrm{sgn}(\lambda_{des}-\lambda_i)+k(\lambda_{des}-\lambda_i)\right] \tag{24}$$

It should be noted again, since the motor braking torque is only acted on the front axle, T_{bi} is the sum of the hydraulic braking torque T_{hf} and the motor braking torque T_{mf} for the front wheel, and for the rear wheel, T_{bi} only equals to hydraulic braking torque T_{hr}.

In order to evaluate stability, the following Lyapunov function is selected:

$$V = (\lambda_{des} - \lambda_i)^2 \tag{25}$$

clearly, $V > 0$.

The differentiation of V is:

$$\dot{V} = 2(\lambda_{des} - \lambda_i)(\dot{\lambda}_{des} - \dot{\lambda}_i) \tag{26}$$

Substituting Equation (18) into above equation gives:

$$\dot{V} = 2(\lambda_{des}-\lambda_i)\left[\dot{\lambda}_{des} - \frac{R}{J_{\omega i}}\frac{1}{v}T_{bi} - \frac{R}{J_{\omega i}}\frac{1}{v}T_{fi} + \frac{R^2}{J_{\omega i}}\frac{1}{v}F_{bi} + \frac{R\omega_i}{v^2}\frac{1}{m}\sum F_{bi} + \frac{R\omega_i}{m}\cdot C_a + \frac{R\omega_i}{mv^2}F_f\right] \tag{27}$$

Again, inserting Equation (24) into Equation (27) and simplifying give:

$$\dot{V} = -2(\lambda_{des}-\lambda_i)\left[\varepsilon\,\mathrm{sgn}(\lambda_{des}-\lambda_i)+k(\lambda_{des}-\lambda_i)\right] \tag{28}$$

It can be proved, that Equation (28) satisfies the sliding condition $\dot{V} < 0$ whenever $(\lambda_{des} - \lambda_i)$ reverses its sign. Therefore, the system is asymptotically stable.

3.2. Parameter Optimizing by Fuzzy Logic Control

For a continuous time system, SMC with exponential reaching law has two adjustable parameters ε and k. The rational selection of both parameters can ensure rapidly reaching and chattering control. The parameter ε is a factor representing the robustness of the system against the disturbance. The larger the parameter ε is, the stronger robustness of the system is. However, the larger parameter ε will also cause severe chatting phenomenon at the same time. Therefore, a suitable choice of parameter set becomes crucial. In this paper, FLC will be used to determine the parameter ε of exponential approach law [20].

A Mamdani fuzzy logic controller with two inputs and one output is designed. The two inputs are the sliding mode function S and the differentiation of the sliding mode function $\dot{S}$, and the output is the parameter ε of exponential approach law. Figure 5 shows the principle of the fuzzy sliding mode controller.
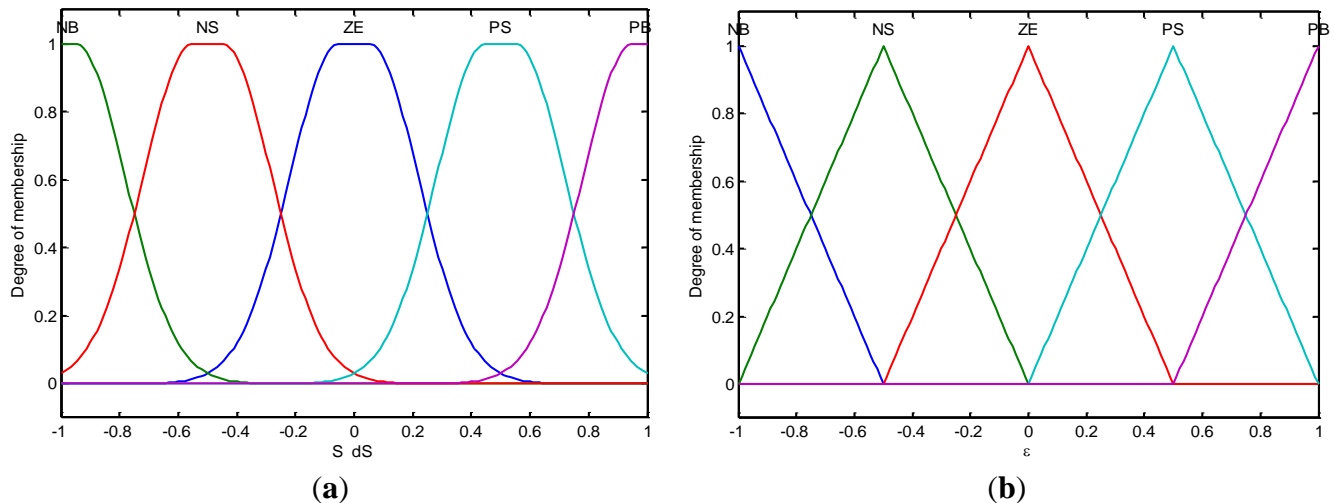
Figure 5. Principle of the fuzzy sliding mode controller (SMC).
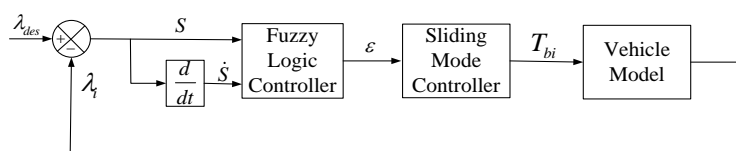
Since $0 \le \lambda_{des}, \lambda_i \le 1$ and $S = (\lambda_{des} - \lambda_i)$, the domain of the input S will be $[-1,1]$. In addition, based on the simulation analysis, the domains of the input $\dot{S}$ and the output ε are also set as $[-1,1]$.

The inputs and output are all divided into five fuzzy subsets: [NB, NS, ZE, PS, PB], where NB, NS, ZE, PM and PB mean negative big, negative small, zero, positive small and positive big, respectively. Gaussian and triangular shapes are selected for the membership functions of the inputs and the output, as shown in Figure 6.

Figure 6. Membership functions for the: (**a**) inputs and (**b**) outputs.

(**a**)

(**b**)

Fuzzy rules have the following form: if *S* is A_i and $\dot{S}$ is B_i, then ε is C_i, where A_i, B_i and C_i are linguistic variables. The fuzzy rules are listed in Table 2.

Table 2. Rules of the fuzzy logic controller. NB, NS, ZE, PM and PB mean negative big, negative small, zero, positive small and positive big, respectively.

ε		*S*				
		NB	**NS**	**ZE**	**PS**	**PB**
	NB	NB	NB	NS	ZE	ZE
	NS	NB	NS	ZE	ZE	ZE
$\dot{S}$	ZE	NS	ZE	ZE	ZE	ZE
	PS	NS	ZE	ZE	PS	PS
	PB	ZE	ZE	PS	PB	PB

Defuzzification of the output is accomplished by the gravity center defuzzifier:

$$y = \frac{\sum_{i=1}^{n} k_i u_i}{\sum_{i=1}^{n} k_i} \tag{29}$$

where k_i is the weight of the *i*th rule; and *n* is the number of rules.
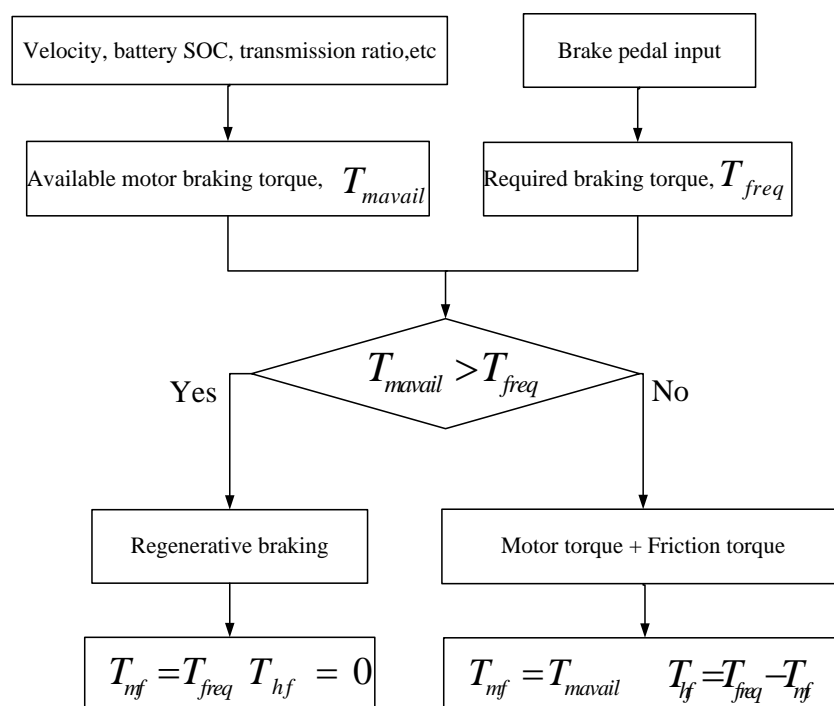
4. Regenerative Braking Algorithm

As stated in Section 2.3, the motor braking torque is limited by several factors. Therefore, regenerative braking must be carried out together with the friction braking in EVs. For the brake

system of EVs, an algorithm is required to decide on how to distribute the braking force between regenerative braking and friction braking in normal braking or emergency braking situations.

As an actuator of braking, the motor not only can convert the braking energy, but also has rapid and precise torque response, which is crucial for ABS. Therefore, from the viewpoints of increasing energy utilization efficiency and improving ABS performance, the motor braking torque should be used to the full extent.

Based on the above goals, for the front wheel, the regenerative braking algorithm shown in Figure 7 is adopted. During emergency braking, on the one hand, the required braking torque is calculated according to Equation (23) or (24); on the other hand, the available motor braking torque is decided depending on various input parameters as illustrated in Section 2.3. If the available motor braking torque T_{mavail} is less than the required braking torque T_{freq}, then both the motor and friction brake system will work in union. The motor braking torque will be used to its maximum level. The difference between the required braking torque and the actual motor torque will be provided by friction brake system. If the available motor braking torque T_{mavail} is more than the required braking torque, then only motor brake will carry out the job, and the motor controller regulates the current input to ensure the required braking torque.

Figure 7. Flow diagram of regenerative braking. *SOC*: state of charge.

For the rear wheel, the required braking torque T_{rreq} will be carried out by friction brake system only. The hydraulic brake controller regulates the wheel cylinder pressure so that the required braking torque is fulfilled.

5. Simulation and Discussion

To evaluate the performance of the proposed SMC and different actuator, simulations were implemented in MATLAB/SIMULINK. Most of the model parameters used in the simulations are

listed in Table 3. The vehicle was brought to a steady longitudinal velocity of 25 m/s (90 km/h) along a straight path and then the ABS was applied on the wheel. Since many researchers have proposed various algorithms about the estimation of the optimal slip ratio, to simplify the problem, the optimal slip ratio 0.2 will be adopted in simulations. The simulations include two parts: one is to compare the brake performance between the Bang-bang and the proposed SMC ABS controller, and between the proposed SMC ABS controller with and without optimizing parameter; the other is to verify the validity of the algorithm about braking torque allocation and compare the brake performance when the motor and the hydraulic brake were used as actuators.

Table 3. Simulation parameters.

Motor	T_{mmax}	150 N·m
	P	32 kW
Vehicle	m	1370 kg
	R, J_w	0.33 m, 3.5 kg·m^2
	L, L_f, L_r, h_g	2.78 m, 1.11 m, 1.67 m, 0.54 m
	C_a, F_f	0.2921, 201.39 N
	i_0, η_t	4.1, 0.95
Tire	C_1	1.029
	C_2	17.16
	C_3	0.523
	C_4	0.03

## *5.1. Comparison of Bang-Bang and Sliding Mode Controller Anti-Lock Braking System Controller*

In this part, simulations were carried out with the Bang-bang and the proposed SMC ABS controller during emergency braking. The simulation results are shown in Figure 8. Figure 8a,b shows the wheel speed and vehicle velocity with the both ABS controller, and Figure 8c illustrates the comparison of the slip ratio of the front wheel. As can be seen, the Bang-bang controller and the proposed SMC controller try to stop the car quickly and keep the slip ratio at the optimal value, and the variation of the vehicle velocity with the SMC ABS is similar to the Bang-bang controller. At the beginning period of braking, due to the initial conventional braking, there is a similar sharp fall of the rotational speed with the two controllers. However, when the slip ratio reaches the optimal value 0.2 and the controller truly takes effect, the differences begin to appear. Comparing to the Bang-bang ABS system, the SMC controller produces smoother variation in wheel rotational speed and the slip ratio, thereby improving braking stability and passenger comfort. The performance of the ABS with the proposed SMC controller is far better than the ones with the Bang-bang based controller.

Figure 9 illustrates the comparison of slip ratio tracking and the actual torque acting on the front wheel of the proposed SMC ABS controller with and without optimizing parameter by FLC. As shown in Figure 9a, the tracking error is smaller and the slip ratio varies more smoothly after the parameter optimizing. The smaller torque fluctuation can also be seen from the comparison of the actual braking torque acting on the front wheel, as shown in Figure 9b. Thus, by the parameter optimizing, the performance of the proposed SMC has been improved obviously, and the chatting phenomenon has been reduced effectively.

Figure 8. Comparison of: (**a**) wheel speed with Bang-bang controller; (**b**) wheel speed with the proposed SMC controller; and (**c**) slip ratio with Bang-bang and the proposed SMC controller.


(**a**)

(**b**)

(**c**)
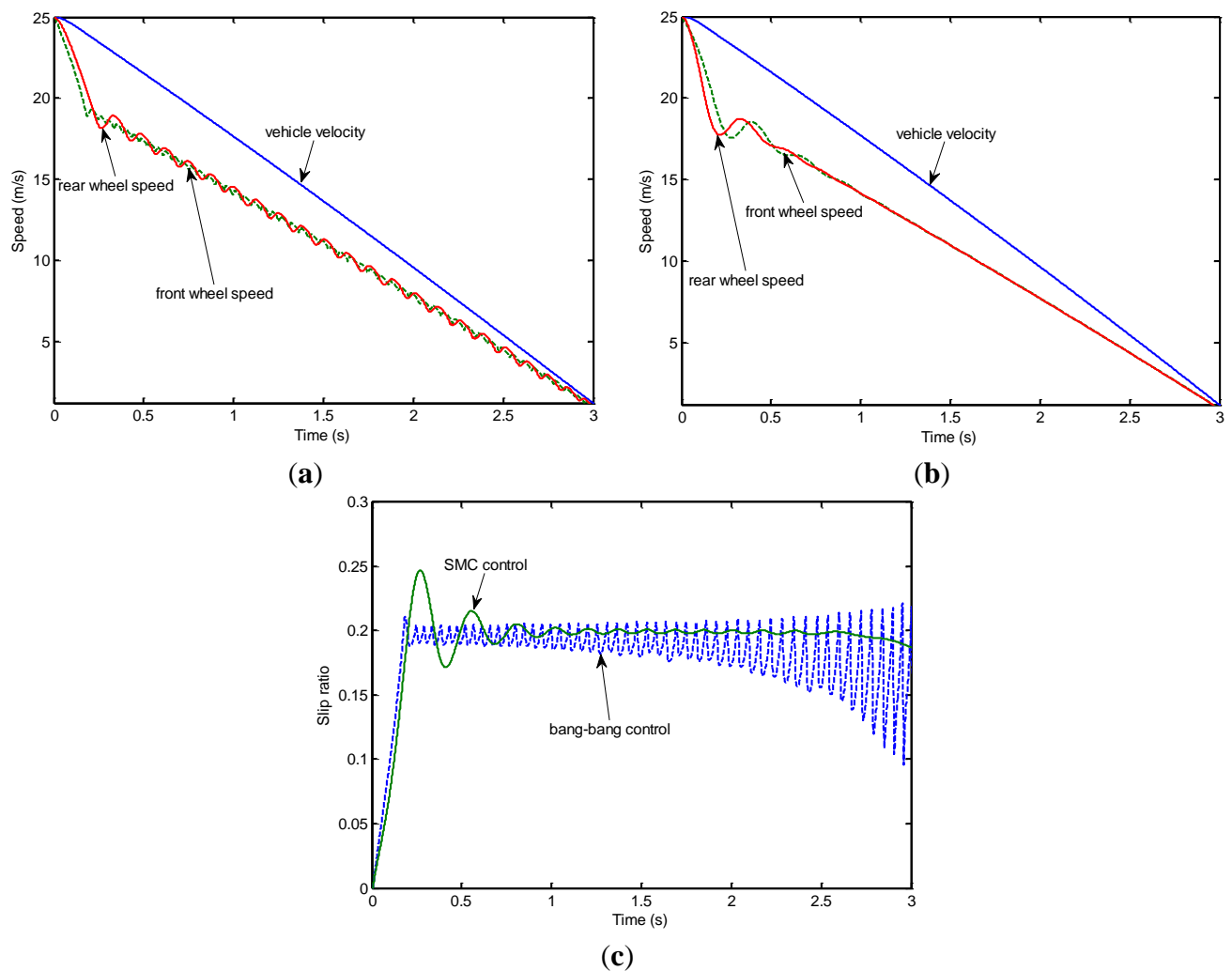
Figure 9. Comparison of: (**a**) slip ratio with the proposed SMC controller with and without optimizing parameter; and (**b**) actual braking torque acting on the front wheel with the proposed SMC controller with and without optimizing parameter.

(**a**)

(**b**)
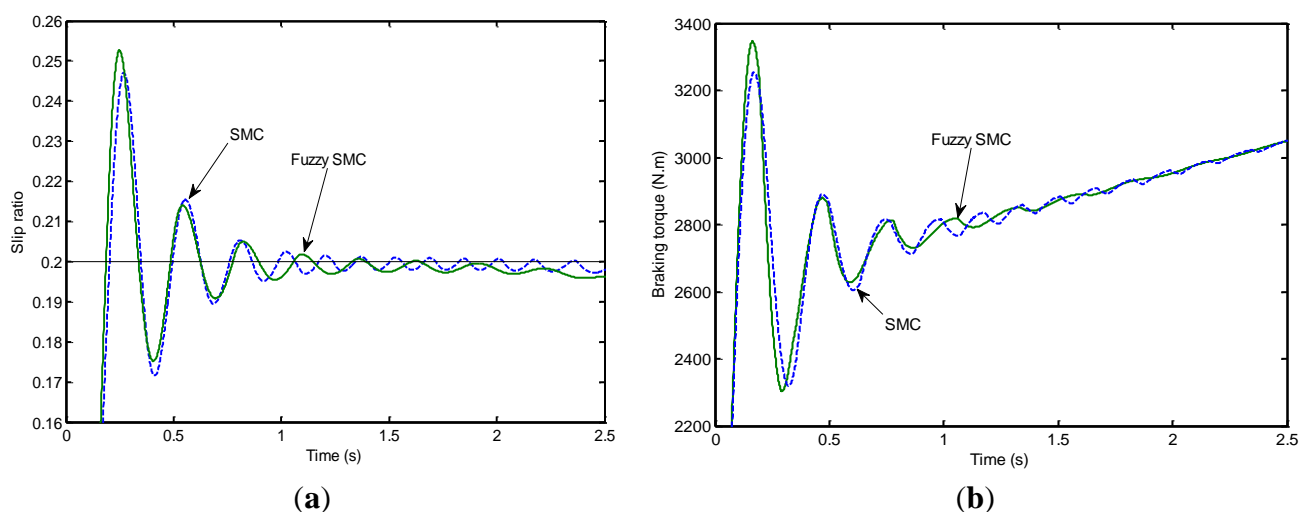
5.2. Validation of Regenerative Braking Algorithm and Comparison of Different Actuator

In order to verify the braking torque allocation and compare the brake performance when the motor and the hydraulic brake were used as actuators, three simulations were performed. One case is to control the motor braking torque zero and ABS will work on the hydraulic brake completely, which is expressed as H-ABS. The second is that the motor and the hydraulic brake work in coordinated control mode under the parameters listed in Table 3, which is expressed as HM-ABS. Finally, the third case is to assume that the maximum motor torque is increased to five times value that listed in Table 3 and the ABS will mainly work on the motor brake, which is expressed as M-ABS. The distributions of braking torque under above three cases are shown in Figure 10.

Figure 10. Distribution of braking force in cases: (**a**) H-ABS; (**b**) HM-ABS; and (**c**) M-ABS.
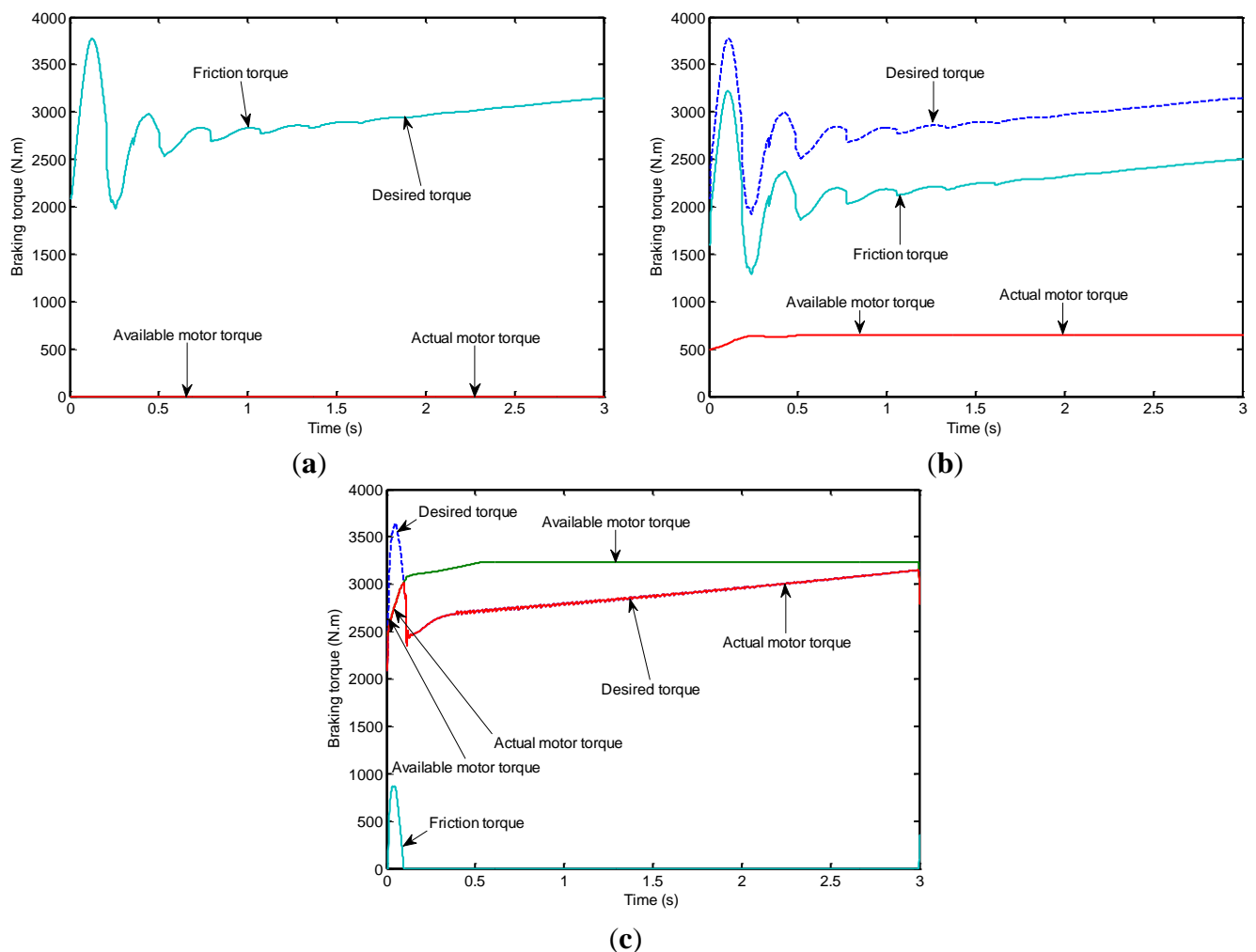

As can be seen from the Figure 10, the available motor braking torque, the actual motor torque both are zero during braking in the case H-ABS. The required braking torque of front wheel is supplied by hydraulic brake completely. In the case HM-ABS, the motor braking torque always keep to its maximum level since the motor torque is small and cannot meet the torque command, and the hydraulic brake system will make up the difference. During the time 0–0.21 s, the motor torque is limited by the motor maximum power, and after the time 3.02 s, the torque is affected by the motor

speed again, as illustrated in Figure 3 and Equation (11). In fact, the ABS algorithm works on the friction brake system in the cases HM-ABS and H-ABS. However, in the case M-ABS, the motor torque is large enough to meet the demand on the front wheel except for the beginning. Therefore, the ABS algorithm mainly works on the motor brake. When the motor torque cannot meet the required torque, the friction brake torque will make up the difference, as shown in Figure 10c. The motor torque is regulated rapidly according to the ABS control algorithm.

As mentioned in Section 2.3, comparing to the traditional friction brake system, the motor has a fast dynamics response characteristic, which will improve the ABS performance. The fact is verified by the comparison of the slip ratio (Figure 11) in the above three cases. As shown in Figure 11, the tracking of the slip ratio under the case M-ABS is the most rapid and accurate in the three cases. The case H-ABS is the worst, but it is also very good with the proposed SMC controller. The case HM-ABS and H-ABS have similar tracking trend since the motor braking torque is smaller than the friction torque in the case HM-ABS and the slip tracking is affected mainly by the friction brake system, as shown in Figure 10b. Besides the excellent torque response, the braking energy can also be converted when the motor is used as actuator. Although more importance should be placed on the stopping distance than the conversion energy in the emergency situation, it is not always a bad thing that the energy efficiency (the ratio between the conversion energy of the motor and the total braking energy of the vehicle) is improved under the condition that the stopping distance is guaranteed.

Figure 11. Comparison of slip ratio in three cases.
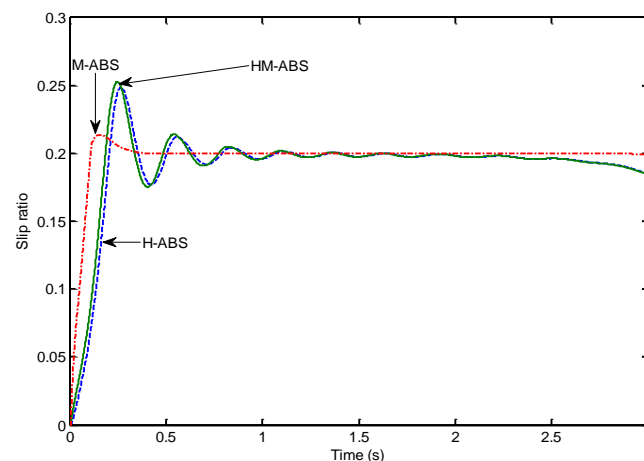
The comparison of stopping distance and conversion energy of above three cases is listed in Table 4. Clearly, compared to the other two cases, in the case M-ABS, the stopping distance is the shortest and the conversion energy is the most. Therefore, under permitted conditions, the motor should be made of the best materials. Of course, in some conditions, compromise for the stopping distance and the conversion energy must be made. Because of the limitation of length, no details will be present here.

Table 4. Stopping distance and conversion energy in three cases.

Braking case	Stopping distance (m)	Conversion energy (kJ)	Energy efficiency
H-ABS	41.12	0	0
HM-ABS	40.88	52.8	12.33%
M-ABS	40.32	175.45	40.98%

6. Conclusions

In this paper, a SMC based on exponential reaching law of the ABS for EVs was put forward. FLC was applied to the reaching law for the selection of parameters. Aiming to make the best of the motor braking torque, a distribution algorithm for braking torque was established. Simulation models of vehicle, actuators and controller were set up in MATLAB/SIMULINK. The simulation results show that, compared with a conventional Bang-bang ABS controller, the braking performance of the vehicle has been improved with the proposed SMC controller. Through the parameter optimization of the reaching law by FLC, the quality for control is improved, and the chattering phenomenon is reduced effectively. Coordinated control has been realized between the motor and the hydraulic brake system. The results also verified that the motor is very suitable to be used as actuator for braking.

Author Contributions

Jingang Guo and Xiaoping Jian built the model of vehicle, tire, motor and hydraulic brake system. Jingang Guo developed the SMC and regenerative braking algorithm. All authors carried out simulation analysis, discussed the simulation results and contributed to writing the paper.

Conflicts of Interest

The authors declare no conflict of interest.

References

1. Sergio, M.S.; Mara, T. *Active Braking Control Systems Design for Vehicles*; Springer: London, UK, 2010; pp. 3–17.
2. Peng, D.; Zhang, Y.; Yin, C.L.; Zhang, J.W. Combined control of a regenerative braking and antilock braking system for hybrid electric vehicles. *Int. J. Automot. Technol.* **2008**, *9*, 749−757.
3. Xu, G.Q.; Li, W.M.; Xu, K.; Song, Z.B. An intelligent regenerative braking strategy for electric vehicles. *Energies* **2011**, *4*, 1461−1477.
4. Long, B.; Lim, S.T.; Ryu, J.H.; Chong, K.T. Energy-regenerative braking control of electric vehicles using three-phase brushless direct-current motors. *Energies* **2014**, *7*, 99–114.
5. Tur, O.; Ustun, O.; Tuncay, R.N. An introduction to regenerative braking of electric vehicles as anti-lock braking system. In Proceedings of the 2007 IEEE Intelligent Vehicles Symposium, Istanbul, Turkey, 13–15 June 2007; pp. 944–948.

6. Bera, T.K.; Bhattacharyya, K.; Samantaray, A.K. Bond graph model based evaluation of a sliding mode controller for combined regenerative and antilock braking system. *Proc. Inst. Mech. Eng. Part I J. Syst. Control Eng.* **2011**, *225*, 918–934.

7. Mirzaei, A.; Moallem, M.; Dehkordi, B. Design of an optimal fuzzy controller for antilock braking systems. *IEEE Trans. Veh. Technol.* **2006**, *55*, 1725–1730.

8. Lin, C.M.; Hsu, C.F. Neural-network hybrid control for antilock braking systems. *IEEE Trans. Neural Netw. Learn. Syst.* **2003**, *14*, 351–359.

9. Yu, J.S. A robust adaptive wheel-slip controller for antilock brake system. In Proceedings of the 36th IEEE Conference on Decision and Control, San Diego, CA, USA, 10–12 December 1997; Volume 3, pp. 2545–2546.

10. Sakai, S.; Sado, H.; Hori, Y. Anti-skid control with motor in electric vehicle. In Proceedings of the 6th International Workshop on Advanced Motion Control, Nagoya, Japan, 30 March–1 April 2000; pp. 317–322.

11. Mi, C.; Lin, H.; Zhang, Y. Iterative learning control of antilock braking of electric and hybrid vehicles. *IEEE Trans. Veh. Technol.* **2005**, *54*, 486–494.

12. Zhou, Z.; Mi, C.; Zhang, G. Integrated control of electromechanical braking and regenerative braking in plug-in hybrid electric vehicles. *Int. J. Veh. Des.* **2012**, *58*, 223–239.

13. Anwar, S. Anti-lock braking control of a hybrid brake-by-wire system. *Proc. Inst. Mech. Eng. Part D J. Automob. Eng.* **2006**, *220*, 1101–1117.

14. Wong, J.Y. *Theory of Ground Vehicles*, 4th ed.; John Wiley & Sons: New York, NY, USA, 2008; pp. 203–288.

15. Pacejka, H.B.; Bakker, E. The magic formula tyre model. *Veh. Syst. Dyn. Int. J. Veh. Mech. Mobil.* **1993**, *21*, 1–18.

16. Oudghiri, M.; Chadli, M.; Hajjaji, A.E. Robust fuzzy sliding mode control for antilock braking system. *Int. J. Sci. Tech. Autom. Control* **2007**, *1*, 13–28.

17. Markel, T.; Brooker, A.; Hendricks, T. ADVISOR: A systems analysis tool for advanced vehicle modeling. *J. Power Sources* **2002**, *110*, 255–266.

18. Wang, W.Y.; Li, I.H.; Tsai, C.P.; Su, S.F.; Hsu, S.B. Dynamic slip-ratio estimation and control of antilock braking system using an observer-based direct adaptive fuzzy–neural controller. *IEEE Trans. Ind. Electron.* **2009**, *56*, 1746–1756.

19. Kim, J.; Lee, J. Real-time estimation of maximum friction and optimal slip ratio based on material identification for a mobile robot on rough terrain. In Proceedings of the 2013 13th International Conference on Control, Automation and Systems (ICCAS), Gwangju, Korea, 20–23 October 2013; pp. 1708–1713.

20. Jiang, K.; Zhang, J.G.; Chen, Z.M. A new approach for the sliding mode control based on fuzzy reaching law. In Proceedings of the 4th World Congress on Intelligent Control and Automation, Shanghai, China, 10–14 June 2000; Volume 1, pp. 656–660.